Multispectral fluorescence imaging to assess pH in biological specimens

Matthew R. Hight,[a,b,*] **Donald D. Nolting,**[b,c,*] **Eliot T. McKinley,**[b,d] **Adam D. Lander,**[d] **Shelby K. Wyatt,**[b,c] **Mark Gonyea,**[e,f] **Ping Zhao,**[b] and **H. Charles Manning**[b,c,d,e,g]

[a]Vanderbilt University, Department of Physics, Astronomy Department, Interdisciplinary Materials Science Program, Nashville, Tennessee 37221
[b]Vanderbilt University Medical Center, Vanderbilt University Institute of Imaging Science, Nashville, Tennessee 37232
[c]Vanderbilt University Medical Center, Department of Radiology and Radiological Sciences, Nashville, Tennessee 37232
[d]Vanderbilt University, Department of Biomedical Engineering, Nashville, Tennessee 37235
[e]Vanderbilt University, Bioengineering Research Experiences for Teachers Program, Nashville, Tennessee 37235
[f]Smyrna High School, Smyrna, Tennessee 37167
[g]Vanderbilt University Medical Center, Program in Chemical and Physical Biology, Nashville, Tennessee 37232

Abstract. Simple, quantitative assays to measure pH in tissue could improve the study of complicated biological processes and diseases such as cancer. We evaluated multispectral fluorescence imaging (MSFI) to quantify extracellular pH (pH_e) in dye-perfused, surgically-resected tumor specimens with commercially available instrumentation. Utilizing a water-soluble organic dye with pH-dependent fluorescence emission (SNARF-4F), we used standard fluorimetry to quantitatively assess the emission properties of the dye as a function of pH. By conducting these studies within the spectroscopic constraints imposed by the appropriate imaging filter set supplied with the imaging system, we determined that correction of the fluorescence emission of deprotonated dye was necessary for accurate determination of pH due to suboptimal excitation. Subsequently, employing a fluorimetry-derived correction factor (C_F), MSFI data sets of aqueous dye solutions and tissuelike phantoms could be spectrally unmixed to accurately quantify equilibrium concentrations of protonated (HA) and deprotonated (A^-) dye and thus determine solution pH. Finally, we explored the feasibility of MSFI for high-resolution pH_e mapping of human colorectal cancer cell-line xenografts. Data presented suggest that MSFI is suitable for quantitative determination of pH_e in *ex vivo* dye-perfused tissue, potentially enabling measurement of pH across a variety of preclinical models of disease. © *2011 Society of Photo-Optical Instrumentation Engineers (SPIE)*. [DOI: 10.1117/1.3533264]

Keywords: pH; imaging; multispectral; fluorescence; tumor.

Paper 10324R received Jun. 11, 2010; revised manuscript received Nov. 1, 2010; accepted for publication Nov. 17, 2010; published online Jan. 24, 2011.

1 Introduction

In normal mammalian tissues, intracellular and extracellular pH (pH_i and pH_e, respectively) are dynamically regulated by a variety of sophisticated mechanisms.[1] For example, pH_i is maintained by both ion-exchange mechanisms and cytosolic buffering capacity. Within this context, pH_i plays important roles in numerous physiological processes, such as protein synthesis and the regulation of cell cycles. Similarly, pH_e is controlled by mechanisms that include vascular delivery of physiological buffers and removal of lactic acid. Although the observed pH_e varies across tissues of differing origin and function, deviation from normal pH_e for a given tissue coincides with a variety of important pathological states (e.g., renal failure, ischemia, chronic pulmonary disease, and cancer).[1] In highly metabolic tissues, such as tumors, reduced pH_e can result from elevated production and diminished removal of lactic acid combined with the reduced capability of tumor-associated vasculature to deliver blood-based pH buffers.[2] Acidic tumor

pH_e can impart significant consequences on cancer cells, such as increased potential for invasion and likelihood of metastasis, although further elucidation of the role of pH within this setting is needed.[3] For these reasons, there is considerable interest in the development and validation of novel methods capable of measuring pH in biological specimens.

The majority of tools currently available for measurement of pH in tissues tend to be invasive (e.g., microelectrodes)[4] and/or provide relatively modest spatiotemporal resolution (e.g., magnetic resonance imaging and magnetic resonance spectroscopy).[1,5] Limitations of the former techniques result from the inability to determine spatially resolved pH gradients without significant damage to the specimen.[2] The latter methods are noninvasive but significantly more costly and complicated to implement, limiting sample throughput and requiring highly specialized equipment and technical expertise.[1,5] In contrast, optical imaging techniques offer an attractive alternative to the aforementioned techniques as they tend to be noninvasive, comparatively simple, analytically sensitive, cost-effective, and rapid.[6–8] The most common optical methods rely on ratiometric fluorescence approaches. In typical assays utilizing exogenous organic dyes such as fluorescein as an indicator, a

---

pH-sensitive excitation/emission combination is compared to a pH-insensitive reference combination.[2,9,10] Alternately, pH-sensitive dyes such as members of the seminaphthorhodafluor (SNARF) family can be excited at a single wavelength and emission collected at multiple wavelengths corresponding to the discrete spectra of protonated (HA) and deprotonated (A$^-$) species in solution.[11–15] Though ratiometric approaches are routine for solution analysis[11] and flow cytometry,[12–14] others have elegantly adapted ratiometric assays to intravital microscopy and demonstrated imaging of interstitial pH gradients in normal and neoplastic tissues in preclinical studies.[2] An inherent limitation of these approaches, which is mitigated somewhat through emission filtering at the expense of signal rejection, is the difficulty of deconvolving multiple fluorescence emissions (i.e., signal versus reference or HA versus A$^-$) due to spectral overlap. Multispectral fluorescence imaging (MSFI) is a well-established technique that is suitable for the separation of multiple distinct, yet spectrally overlapping emissions.[16] When utilized in preclinical animal studies, separation and quantification of multiple fluorescence emissions from imaging probes is feasible.[17–20] Paired with pH-sensitive fluorochromes that generate unique emission spectra for HA and A$^-$ species, MSFI potentially represents an ideal paradigm for measurement of pH in solution and/or in tissue. Additionally, MSFI systems suitable for use in preclinical animal studies or in conjunction with microscopy are now readily available and relatively inexpensive.

In these studies, we illustrate a simple, rapid approach to quantitatively assess pH$_e$ in dye-perfused biological tissues utilizing MSFI and commercially available instrumentation. Using the MSFI-based approach, we demonstrate the feasibility of mapping pH$_e$ gradients pertaining to the protonation and deprotonation equilibrium of the pH-sensitive dye SNARF-4F in tissue specimens. It is anticipated that this methodology will provide valuable information regarding *ex vivo* tumor pH$_e$ and will ultimately aid in the study of the relationship between tumors and tumor microenvironments, as well as the effect of therapeutic regimens on tumor pH$_e$.

2 Materials and Methods

2.1 Chemicals

All chemicals, reagents and solvents were purchased from indicated suppliers and used without further purification: SNARF-4F 5-(and-6)-carboxylic acid (Invitrogen; Carlsbad, California), American Chemical Society (ACS)-grade hydrochloric acid (HCl) (EMD; Gibbstown, New Jersey), ACS-grade sodium hydroxide (NaOH) (Fisher Scientific; Pittsburgh, Pennsylvania), laboratory-grade gelatin from porcine skin, type A (Sigma Aldrich; Milwaukee, Wisconsin), bovine hemoglobin (Sigma Aldrich; Milwaukee, Wisconsin), and intralipid 20% (Fresenius Kabi AB).

2.2 Aqueous pH Solutions

Solutions ranging from pH 3–10 in 0.5-pH increments were prepared from a 1.0-μM aqueous stock solution of SNARF-4F separated into 10-mL aliquots. The pH of each aliquot was adjusted via microadditions of concentrated HCl and/or NaOH.

Solution pH adjustments were monitored with a calibrated pH meter (MP220 pH Meter, Mettler Toledo, Columbus, OH) under positive nitrogen pressure with vigorous stirring. Over the course of the experiment, the solutions were wrapped in aluminum foil to minimize light exposure. Spectroscopic analysis and/or MSFI of pH-adjusted samples were performed immediately following pH adjustment and stabilization.

2.3 Preparation of Biological Phantoms

To validate the ability of MSFI to measure pH in biological environments, tissuelike phantoms with the approximate photon scattering and absorption properties of biological tissues were prepared.[21] First, a 10% gelatin solution was prepared by adding gelatin to heated deionized water (40–50°C) with constant stirring. The solution was then cooled to 30–40°C, at which the desired amounts of bovine hemoglobin and intralipid were added, resulting in a 42.5-μM hemoglobin and 1% intralipid phantom mixture. Three parts buffered dye solution [acetate buffer (pH 4.3, 5.6), phosphate buffer (pH 6.2, 7.3), tris-HCl buffer (pH 8.4), and carbonate buffer (pH 9.5)] and one part phantom mixture were combined and dispensed into a chilled well plate and refrigerated at 4°C until solid.

2.4 Fluorimetry

The spectroscopic characteristics of pH-adjusted aqueous SNARF-4F solutions were investigated using a Photon Technology International QuantaMaster$^{\text{TM}}$ 50 fluorimeter (Birmingham, New Jersey) and a standard, 1-cm path-length quartz cuvette (NSG Precision Cells 517BES10). An excitation wavelength (λ_{ex}) of 523 nm was used for single-wavelength studies, whereas an excitation range of 425–650 nm in increments of 25 nm was used for multiple-wavelength studies. Emission scans were collected every nanometer over the emission wavelength (λ_{em}) range of 400–800 nm with an integration time of 0.1 s and a shutter width of 1.5 nm. Three acquisitions were averaged for each λ_{ex}. Excitation emission matrices of fluorescence emission as a function of excitation were generated in MATLAB (The MathWorks, Inc., Natick, Massachusetts). Fluorimetry data were used in conjunction with

$$C_{\text{F}} = \frac{F_{\lambda_2}}{F_{\lambda_1}} \tag{1}$$

to generate a correction factor (C_{F}) that was later applied to the A$^-$ fluorescence intensity obtained in MSFI studies. In Eq. (1), F refers to the fluorescence intensity at 653 nm when excited at 525 nm (λ_1) or 575 nm (λ_2).

2.5 MSFI: Aqueous Solutions

Aqueous SNARF-4F solutions ranging in pH from four to eight in increments of ∼1.0 pH unit were imaged using the Maestro$^{\text{TM}}$ Q FLEX *In Vivo* Imaging System from CRi, Inc. (Woburn, Massachusetts). Solutions were imaged in 1.5-mL microcentrifuge tubes that were prerinsed with pH-adjusted solution prior to addition of dye solution. All images were obtained using Maestro Q Filter Set B, which features a bandpass excitation filter with transmission centered at 525 nm (full width at half

maximum $= 47$ nm) and a long-pass emission filter with 560 nm cut in. A spectral library was generated that included emission spectra for fully protonated/deprotonated dye species as well as autofluorescence from the microcentrifuge tube plastic. This library was used throughout the solution phase experiments for spectral unmixing. Quantitative analysis of the autofluorescence signal arising from the microcentrifuge tubes demonstrated that >95% of the autofluorescence could be removed by spectral unmixing (data not shown). Unmixed dye fluorescence intensity data were obtained from a manually drawn region of interest (ROI) shaped and sized to include the central region of the microcentrifuge tube. The data were fitted to a nonlinear sigmoidal model and plotted against the analytically measured solution pH. Uncorrected and corrected SNARF-4F pK_a values were calculated.

2.6 *MSFI—Biological Phantoms*

Using a protocol similar to that used for the solution phase experiments, dye containing tissuelike phantoms ranging in a pH of 4–9.5 were imaged with the Maestro Q system. Spectral unmixing was achieved by applying the previously derived solution phase spectral library with the inclusion of autofluorescence from tissuelike phantom controls. Unmixed fluorescence intensity data were obtained from an ellipselike manually drawn ROI sized to include the entirety of a single well. The data were fit to a nonlinear sigmoidal model and plotted against the analytically measured solution pH. Uncorrected and corrected SNARF-4F pK_a values were calculated.

2.7 *Ex Vivo pH Mapping of Human Xenograft Tumor Tissue*

All studies involving the use of animal models were conducted in accordance with Vanderbilt University Institutional Animal Care and Use Committee and applicable federal guidelines. To generate the human colorectal cancer (CRC) model used for tumor imaging, 200,000 DiFi human CRC cells were subcutaneously injected on the left flank of athymic nude mice, as previously described.[17] Experiments were conducted two to three weeks postinoculation, when tumors reached ~250 mm³. For pH_e mapping, 1.0 nmol of SNARF-4F in 200 μL of saline was administered to xenograft-bearing mice via intravenous injection under inhalation of anesthesia (2% isofluorane). Following dye administration, mice were allowed to briefly recover from anesthesia and given access to food and water *ad libitum* during a 15-min uptake period. Mice were then sacrificed and tumor tissue harvested. Immediately following collection (<2 min), tumors were macrodissected into two equivalent hemispheres, positioned with the intratumoral facets facing toward the camera, and imaged using the Maestro Q system. Fluorescence images were collected from 560 to 850 nm and unmixed using the previously described spectral library (excluding autofluorescence from plastic). Unmixed fluorescence intensity data were obtained from a manually drawn ROI (~2% of the total area) that was applied to multiple areas of the tumor in order to ascertain pH heterogeneity. A gradient pH_e map was generated in
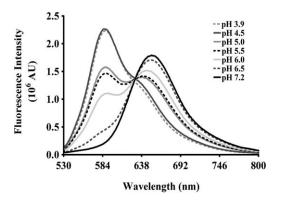

Fig. 1 Combined fluorescence emission spectra (excitation 523 nm) of aqueous SNARF-4F samples ranging in pH from ~4 to 7. The emission spectrum of pH 3.9 is representative of subsequently decreasing pH values (data not shown) while the emission spectrum of pH 7.2 is representative of subsequently increasing pH values (data not shown).

MATLAB from each MSFI unmixed image using

$$pH = pK_a - \log\left(\frac{C_F S_{A^-}}{S_{HA}}\right). \qquad (2)$$

Here, pK_a is that of the dye while S_{A^-} and S_{HA} correspond to the observed fluorescence intensity of each species, respectively.

3 Results and Discussion

3.1 *Spectroscopy*

The fluorescence spectroscopy of the SNARF family of organic dyes is dependent on the protonation state of the compound. Typically, the protonated and deprotonated states of the compound yield distinct, yet overlapping, emission peaks that may be separated by as much as 60 nm.[22] For these studies, aimed at measuring pH in tissue, an important determinant was selection of a dye possessing a pK_a near the anticipated pH of the specimens being assayed. These studies utilized SNARF-4F, with a known pK_a of 6.4. Thus, at pH values well below its pK_a, the dye exists predominately in a protonated state and exhibits fluorescence emission at 580 nm when excited at 523 nm (Fig. 1). SNARF-4F exists in a predominately deprotonated state at pH values well above the pK_a and exhibits fluorescence emission at 640 nm when excited at 523 nm (Fig. 1). Importantly, across the physiologically relevant pH range of 5–7, both HA and A^- species exist in equilibrium. Because of the unique emission spectroscopy of the HA and A^- species, spectral unmixing and quantitative measurement of each species facilitate determination of pH in accordance with a modified Henderson–Hasselbalch equation.

Conceptually, the simplest pH imaging study coupling SNARF-4F and the Maestro system would feature utilization of a single excitation band and simultaneous collection and spectral unmixing of both the HA and A^- emissions. However, an important assumption of this approach is the requirement for equivalent excitation and collection of both the HA and A^- species, which may be thought of as two separate fluorophores in this experiment. Because the emission of the A^- species is significantly redshifted (ca. 60 nm) from the HA species,
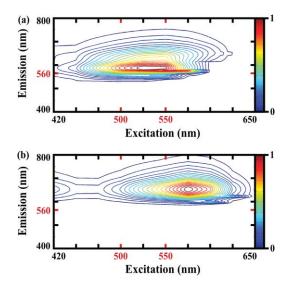
Fig. 2 Excitation emission matrices of SNARF-4F fluorescence emission as a function of excitation wavelength for HA [(a) pH 4.5] and A^- [(b) pH 10.0]. Red marks located along the excitation axis show the approximate bandpass transmission of the Maestro Q B excitation filter, while the red mark on the emission axis shows the cut-on point for the long-pass emission filter. The excitation-emission coordinates for the point at which maximum fluorescence emission intensity is achieved are (525, 587) for (a) and (575, 653) for (b).

Table 1 Observed (uncorrected) and calculated (corrected) pK_a values for different SNARF-4F containing mediums.

Medium	Observed pK_a	Calculated pK_a
Solution	6.7 ± 0.3	6.4 ± 0.2
Phantom	6.7 ± 0.3	6.3 ± 0.4

with minor attenuation ($\sim$5%) of the HA emission from 530 to 560 nm.

To compensate for the suboptimal excitation of the A^- species, a correction factor ($C_F = 2.1 \pm 0.03$) was derived from Eq. (1). Equation (1) defines the ratio of the observed emission intensity at 650 nm for the A^- species when excited at 525 nm (λ_1), the excitation wavelength in the Maestro, compared to the emission intensity at 650 nm when optimally excited at 575 nm (λ_2).

3.2 *MSFI*

To validate C_F for use in MSFI assays, aqueous SNARF-4F solutions with pH values between 4 and 8 and tissuelike phantoms with pH values between 4 and 9.5 were imaged using filter set B and spectrally unmixed using the previously established spectral library. Following spectral unmixing, manual ROIs were drawn on unmixed images corresponding to the HA and A^- species [Figs. 4(a) and 4(b)]. Accordingly, the measured fluorescence intensities for each species were used to calculate the observed, uncorrected pK_a for the dye using a modified Henderson–Hasselbalch equation, substituting the fluorescence emission intensity for each species in place of HA and A^- concentration. Prior to correction of the A^- intensity, fitting the unmixed HA and A^- intensities to a sigmoidal curve and plotting versus pH [Figs. 4(c) and 4(d)] resulted in intersection between the two curves (by definition, pK_a) at 6.7 $\pm$ 0.3 for both the solution phase and biological phantom data (Table 1). Though these observed values are slightly higher than the known pK_a of 6.4,[22] application of the fluorimetry determined C_F to the A^- intensities of all data resulted in indistinguishable calculated pK_a values of $\sim$6.4 (Table 1) using Eq. (2), therefore validating C_F derived from the fluorimetry experiments in multiple mediums.

it follows that equivalent excitation of each species using a common excitation wavelength is unlikely. Therefore, we explored the relationships between excitation wavelength, pH, and the resulting emission spectroscopy of both the HA and A^- SNARF-4F species using standard fluorimetry. We found that the HA species exhibited maximum fluorescence emission at an excitation wavelength of $\sim$525 nm (emission = 590 nm), while the A^- species exhibited maximum fluorescence emission at an excitation wavelength of $\sim$575 nm (emission = 650 nm) (Fig. 2). Optimization of the imaging assay to utilize only a single filter set could be accomplished using a single filter set included with the Maestro system [denoted as "B", bandpass excitation 525/25 nm, long-pass emission 560 nm, (Fig. 3)]. This filter set was ideally suited for exciting the HA species but was suboptimal for exciting the A^- species. We found the long-pass emission filter contained within the B filter set was suitable for simultaneous collection of both the HA and A^- emission,
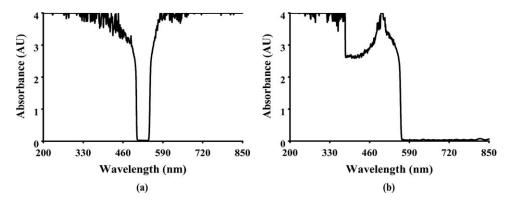

Fig. 3 Transmission spectrum for (a) bandpass excitation filter and (b) long-pass emission filter supplied as Filter Set B with the Maestro Q imaging system.
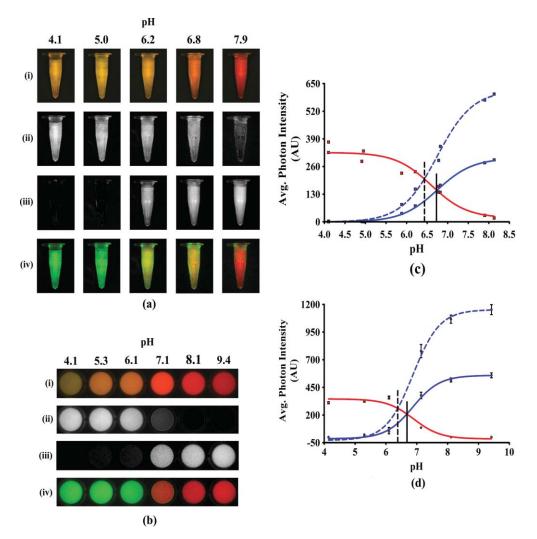
Fig. 4 Multispectral fluorescence imaging of (a) aqueous SNARF-4F solutions ranging in pH from approximately 4 to 8 and (b) dye-containing tissuelike phantoms ranging in pH from approximately 4 to 9.5. Spectrally mixed, pseudocolor composite images are shown in row i of both (a) and (b). Spectrally mixed composite images were unmixed to visualize emission from the HA [row ii of both (a) and (b)] and A$^-$ [row iii of both (a) and (b)] species. Pseudocolor, unmixed composite images are shown in row iv of both (a) and (b), where the HA fluorescence emission is pseudocolorized in green and the A$^-$ fluorescence emission is pseudocolorized in red. Quantified average photon intensities from (a) are given in (c) while intensities from (b) are given in (d). HA (red) and A$^-$ (blue) species are displayed across pH as assessed by MSFI. Nonlinear fits of MSFI data (solid colored lines) result in goodness of fits of 7 (c) and 33 (d) degrees of freedom. Observed pK$_a$ values (Table 1), the pH at which [HA] = [A$^-$], are noted by solid black lines. Correction of the A$^-$ intensity using C_f at each point (dotted blue line) results in calculated pK$_a$ values (noted by dashed black lines) that are equivalent within one standard deviation of one another (Table 1).

Table 2 MSFI-measured photon intensities and calculated pH values for DiFi CRC xenograft tumor. Location for each ROI is shown in Fig. 5(d).

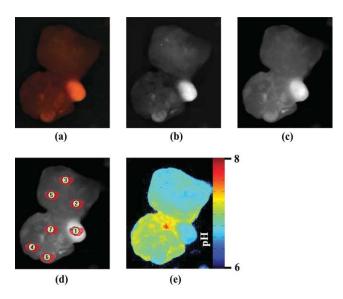| ROI	A$^-$ Photon Intensity	Corrected A$^-$ Photon Intensity	HA Photon Intensity	log(A$^-$/HA)	Estimated pH$_e$
1	454	937	371	0.4	6.8
2	141	290	99	0.5	6.9
3	132	272	98	0.5	6.9
4	139	286	67	0.6	7.0
5	141	290	98	0.5	6.9
6	247	509	162	0.5	6.9
7	190	392	70	0.8	7.2

pHe: range = 6.80–7.2, mean = 6.9 ± 0.1

Fig. 5 MSFI of dye-perfused human CRC cell line xenograft. (a) Spectrally mixed pseudocolor fluorescence image. Spectrally unmixed images show (b) HA and (c) A$^-$ fluorescence emission. (d) Map illustrating the selected ROI placement for pH measurements performed in tumor regions corresponding to the values shown in Table 2. Pixel-by-pixel pH$_e$ map generated using the HA fluorescence emission and the corrected A$^-$ emission (e). Color bar corresponds to the calculated pH in each pixel.

3.3 Ex Vivo pH Mapping of Xenograft Tumors

We next explored utilizing the MSFI approach for spatially resolved determination of pH$_e$ in freshly resected xenograft tumor tissue. Using the Maestro Q system, we observed perfusion of SNARF-4F throughout the entire tumor, though accumulation tended to be heterogeneous [Fig. 5(a)]. Increased levels of accumulation were noted in tissues exhibiting elevated necrosis. Nonuniform accumulation of dye in disorganized tissue such as tumors is not unexpected. It is therefore important to emphasize that the ratiometric nature of the proposed MSFI approach renders pH measurement inherently concentration independent with respect to the dye, provided that detectable quantities are present within tissues of interest. Applying the previously established spectral library for the HA and A$^-$ species to the unmixed data, fluorescence emission of the HA [Fig. 5(b)] and A$^-$ [Fig. 5(c)] species could be visualized within tumor tissue. To quantify intratumoral pH$_e$, the fluorescence intensity for the HA and A$^-$ species was measured by manual ROI analysis [Fig. 5(d)]. The measured intensity of the A$^-$ species was corrected using C_F, and tumor pH$_e$ for each ROI was calculated using Eq. (2) (Table 2). We found that pH$_e$ within the tumor was heterogeneous with a mean pH of 6.9 $\pm$ 0.1. These observations are in agreement with those reported by previous studies where pH$_e$ was assessed across multiple tumor types by alternative techniques.[23–26] Expanding on this, to generate a high-resolution pH map of tumor tissue, the HA and corrected A$^-$ pixel intensities were imported into MATLAB, where the pH was calculated, fit to a color bar, and displayed across each image pixel [Fig. 5(e)]. Although much of the tumor could be considered acidic with respect to normal tissue, we observed that tumor regions exhibiting the lowest pH tended to coincide with the highest degrees of necrosis in this model. These results

suggest the feasibility of MFSI for *ex vivo* measurement of pH$_e$ in preclinical tissue specimens.

4 Conclusions

We report a novel method for simple, rapid measurement of pH$_e$ in biological tissue that utilizes MSFI. Given the ability to assess pH in a spatially resolved manner, this technique could be employed in preclinical research to further elucidate the relationship(s) between the pH of a tumor and its surrounding microenvironment, as well as the role of pH in other preclinical models of disease. We envision that this approach could be most useful when utilized in conjunction with other complementary molecular techniques, such as immunohistochemistry, and deployed immediately following tissue collection and prior to freezing or fixation.

References

1. R. J. Gillies, N. Raghunand, M. L. Garcia-Martin, and R. A. Gatenby, "pH imaging. a review of pH measurement methods and applications in cancers," *IEEE Eng. Med. Biol. Mag.* **23**(5), 57–64 (2004).
2. G. R. Martin and R. K. Jain, "Noninvasive measurement of interstitial pH profiles in normal and neoplastic tissue using fluorescence ratio imaging microscopy," *Cancer Res.* **54**(21), 5670–5674 (1994).
3. R. J. Gillies, N. Raghunand, G. S. Karczmar, and Z. M. Bhujwalla, "MRI of the tumor microenvironment," *J. Magn. Reson. Imaging* **16**(4), 430–450 (2002).
4. S. K. Calderwood and J. A. Dickson, "Effect of hyperglycemia in blood flow, pH, and response to hyperthermia (42 degrees) of the Yoshida sarcoma in the rat," *Cancer Res.* **40**(12), 4728–4733 (1980).
5. N. Raghunand, "Tissue pH measurement by magnetic resonance spectroscopy and imaging," *Methods Mol. Med.* **124**, 347–364 (2006).
6. S. Weiss, "Fluorescence spectroscopy of single biomolecules," *Science* **283**(5408), 1676–1683 (1999).
7. W. P. Ambrose, P. M. Goodwin, J. H. Jett, A. Van Orden, J. H. Werner, and R. A. Keller, "Single molecule fluorescence spectroscopy at ambient temperature," *Chem. Rev.* **99**(10), 2929–2956 (1999).
8. W. E. Moerner and D. P. Fromm, "Methods of single-molecule fluorescence spectroscopy and microscopy," *Rev. Sci. Instrum.* **74**(8), 3597–3619 (2003).
9. S. Ohkuma and B. Poole, "Fluorescence probe measurement of the intralysosomal pH in living cells and the perturbation of pH by various agents," *Proc. Natl. Acad. Sci. U.S.A.* **75**(7), 3327–3331 (1978).
10. L. Tanasugarn, P. Mcneil, G. T. Reynolds, and D. L. Taylor, "Microspectrofluorometry by digital image processing: measurement of cytoplasmic pH," *J. Cell Biol.* **98**(2), 717–724 (1984).
11. N. Marcotte and A. M. Brouwer, "Carboxy SNARF-4F as a fluorescent pH probe for ensemble and fluorescence correlation spectroscopies," *J. Phys. Chem. B* **109**(23), 11819–11828 (2005).

12. P. E. Van Erp, M. J. Jansen, G. J. Jongh, J. B. Boezeman, and J. Schalkwijk, "Ratiometric measurement of intracellular pH in cultured human keratinocytes using carboxy-SNARF-1 and flow cytometry," *Cytometry* **12**(2), 127–132 (1991).

13. E. D. Wieder, H. Hang, and M. H. Fox, "Measurement of intracellular pH using flow cytometry with carboxy-SNARF-1," *Cytometry* **14**(8), 916–921 (1993).

14. J. Bond and J. Varley, "Use of flow cytometry and SNARF to calibrate and measure intracellular pH in NS0 cells," *Cytometry* **64**(1), 43–50 (2005).

15. R. C. Hunter and T. J. Beveridge, "Application of a pH-sensitive fluoroprobe (C-SNARF-4) for pH microenvironment analysis in Pseudomonas aeruginosa biofilms," *Appl. Environ. Microbiol.* **71**(5), 2501–2510 (2005).

16. L. Zhou and W. S. El-Deiry, "Multispectral fluorescence imaging," *J. Nucl. Med.* **50**(10), 1563–1566 (2009).

17. H. C. Manning et al. "Molecular imaging of therapeutic response to epidermal growth factor receptor blockade in colorectal cancer," *Clin. Cancer Res.* **14**(22), 7413–7422 (2008).

18. H. C. Manning, S. D. Shay, and R. A. Mericle, "Multispectral molecular imaging of capillary endothelium to facilitate preoperative endovascular brain mapping," *J. Neurosurg.* **110**(5), 975–980 (2009).

19. S. K. Wyatt, H. C. Manning, M. Bai, S. N. Bailey, P. Gallant, G. Ma, L. McIntosh, and D. J. Bornhop, "Molecular imaging of the translocator protein (TSPO) in a pre-clinical model of breast cancer," *Mol. Imaging Biol.* **12**(3), 349–358 (2010).

20. J. Virostko, J. Xie, D. E. Hallahan, C. L. Arteaga, J. C. Gore, and H. C. Manning, "A molecular imaging paradigm to rapidly profile response to angiogenesis-directed therapy in small animals," *Mol. Imaging Biol.* **11**(3), 204–212 (2009).

21. A. M. De Grand, S. J. Lomnes, D. S. Lee, M. Pietrzykowski, S. Ohnishi, T. G. Morgan, A. Gogbashian, R. G. Laurence, and J. V. Frangioni, "Tissue-like phantoms for near-infrared fluorescence imaging system assessment and the training of surgeons," *J. Biomed. Opt.* **11**(1), 014007 (2006).

22. SNARF-4F (5-(and-6)-carboxylic acid product insert, Invitrogen, Carlsbad, CA, http://probes.invitrogen.com/media/pis/mp01270.pdf, (accessed June 20, 2010).

23. T. Volk, E. Jähde, H. P. Fortmeyer, K. H. Glüsenkamp, and M. F. Rajewsky, "pH in human tumour xenografts: effect of intravenous administration of glucose," *Br. J. Cancer* **68**(3), 492–500 (1993).

24. K. Engin, D. B. Leeper, J. R. Cater, A. J. Thistlethwaite, L. Tupchong, and J. D. McFarlane, "Extracellular pH distribution in human tumours," *Int. J. Hyperthermia* **11**(2), 211–216 (1995).

25. R. Van Sluis, Z. M. Bhujwalla, N. Raghunand, P. Ballesteros, J. Alvarez, S. Cerdán, J. P. Galons, and R. J. Gillies, "In vivo imaging of extracellular pH using 1H MRSI," *Magn. Reson. Med.* **41**(4), 743–750 (1999).

26. A. S. Ojugo, P. M. McSheehy, D. J. McIntyre, C. McCoy, M. Stubbs, M. O. Leach, I. R. Judson, and J. R. Griffiths, "Measurement of the extracellular pH in mice by magnetic resonance spectroscopy: a comparison of exogenous (19)F and (31)P probes," *NMR Biomed.* **12**(8), 495–504 (1999).